Available online at www.sciencedirect.com
SCIENCE DIRECT®
Biomaterials 26 (2005) 7436–7446
Biomaterials
www.elsevier.com/locate/biomaterials

Macroporous interconnected dextran scaffolds of controlled porosity for tissue-engineering applications

Stéphane G. Lévesque[a,c], Ryan M. Lim[a], Molly S. Shoichet[a,b,c,*]

[a]Department of Chemical Engineering and Applied Chemistry, 200 College Street, Toronto, Ont., Canada M5S 3E5
[b]Department of Chemistry, 80 St. George St., Toronto, Ont., Canada M5S 3H6
[c]Institute of Biomaterials and Biomedical Engineering, University of Toronto 4 Taddle Creek Road, Toronto, Ont., Canada M5S 3G9

Available online 14 July 2005

Abstract

Dextran hydrogels have been studied as drug delivery vehicles but not as scaffolds for tissue-engineering likely because previously synthesized dextran hydrogels had pores too small for cell penetration. Our goal was to create macroporous, interconnected dextran scaffolds. To this end, we took advantage of the liquid–liquid immiscibility of poly(ethylene glycol) and methacrylated dextran during radical crosslinking of the methacrylated moieties. By controlling the degree of methacrylate substitution on dextran, dextran molar mass and PEG concentration, macroporous hydrogels were created. The presence of PEG in solution had a significant effect on the final morphology of the dextran hydrogel leading to the formation of different types of structures, from microporous gel to macroporous gel-wall to a macroporous interconnected-beaded structure. A series of formulation diagrams were prepared which allowed us to determine which conditions led to the formation of macroporous interconnected-beaded scaffolds. Dextran macroporous interconnected-beaded gels had a high water content, between 89% and 94%, a homogeneous morphology, determined by scanning electron microscopy, with interconnected macroporous pores, as determined by protein diffusivity where the effective diffusion coefficients of BSA were calculated to be 3.1×10^{-7} cm^2/s for Dex-MA 40 kDa DS 5 and 1×10^{-7} cm^2/s for Dex-MA 6 kDa DS10, which are similar to that of BSA in water, 5.9×10^{-7} cm^2/s. Mercury intrusion porosimetry showed that the macroporous interconnected-beaded scaffolds had a bimodal distribution of macropores, with a median diameter of 41 μm, interconnected by throats, which had a median diameter of 11 μm. Together, these data suggest that the dextran scaffolds will be advantageous in applications that require an interconnected macroporous geometry, such as those of tissue engineering where cell penetration and nutrient diffusion are necessary for tissue regeneration.

Keywords: Hydrogel; Macroporous structure; Methacrylated dextran; Phase diagram; Biomaterials

1. Introduction

Hydrogels derived from either natural or synthetic polymers have been of interest for cell encapsulation [1] and drug delivery [2,3]. In recent years, hydrogels have been investigated for tissue-engineering applications as scaffolds to support and promote the regeneration of tissues [4–6]. The interest in hydrogels for soft tissue applications has increased owing to their capacity to be designed to match the mechanical properties and water content of these tissues. However these physical characteristics are not sufficient for hydrogels to fulfill their role to support and promote tissue growth. For scaffold utility, interconnectivity, porosity and pore size are also important to facilitate cell penetration, nutrient diffusion, and tissue regeneration.

Naturally derived hydrogels include crosslinked proteins, polypeptides and polysaccharides such as: collagen, gelatin, hyaluronate, fibrin, alginate, agarose, and chitosan [7]. For example, alginate [8–12], chitosan [13–15], and collagen [16] have been investigated in tissue-engineering applications as cell carriers and scaffolds.

*Corresponding author. Institute of Biomaterials and Biomedical Engineering, University of Toronto 4 Taddle Creek Road, Toronto, Ont., Canada M5S 3G9. Tel.: +1 416 978 1460; fax: +1 416 978 4317.
E-mail address: molly@ecf.utoronto.ca (M.S. Shoichet).

0142-9612/$ - see front matter © 2005 Elsevier Ltd. All rights reserved.
doi:10.1016/j.biomaterials.2005.05.054

Dextran, a bacterial-derived polysaccharide, consists essentially of α-1,6 linked D-glucopyranose residues with a few percent of α-1,2-, α-1,3-, or α-1,4-linked side chains. Dextran particles have been widely used as separation matrices [17–20], such as Sephadex®, as cell microcarriers when surface modified [21–23], such as Cytodex™, and more recently as drug delivery vehicles [24]. We were interested in studying dextran as a scaffold for tissue-engineering applications because we thought that we could take advantage of the liquid–liquid phase separation observed in microsphere processing for scaffold design.

Dextran hydrogels can be created by either physical or chemical crosslinking, taking advantage of the hydroxyl groups present on the α-1,6-linked D-glucose residues. Dextran was physically crosslinked after derivatization with L-lactic acid and D-lactic acid oligomers [25]. Chemical hydrogels were obtained by covalently crosslinking dextran with bifunctional isocyanates [26], glutaraldehyde [27], or by partial oxidation of dextran hydroxyl groups to aldehydes that were then crosslinked with gelatin [28,29]. Alternatively, dextran hydrogels have been synthesized by radical polymerization of derivatized dextran with polymerizable groups. Edman et al. introduced polymerizable moieties to dextran by derivatizing it with glycidyl acrylate under aqueous conditions [30]. Similar studies have been achieved using a diversity of polymerizable groups including: (meth)acrylates [31,32], allyl isocyanate [33], maleic anhydride [32], or vinyl acrylate using a chemo-enzymatic procedure [34]. More recently, Hennink and co-workers described how to control the degree of substitution (DS, the number of methacrylate groups per 100 glucopyranose residues) of methacrylated groups on dextran using one of glycidyl methacrylate (GMA) [35,36], hydroxyethyl methacrylate (HEMA) [37], or lactate-HEMA [37]. Hydrogels obtained with dextran derivatized with glycidyl methacrylate (Dex-GMA) were shown to be stable under physiological conditions [38] and biocompatible in vivo [39] whereas hydrogels of Dex-HEMA or Dex-lactate-HEMA were susceptible to hydrolysis [38].

Dextran hydrogel scaffolds are particularly compelling as scaffolds for soft tissue-engineering applications because dextran has been shown to be resistant to both protein adsorption and cell adhesion [40–42] allowing one to design a scaffold with specific sites for cell recognition [42], as has been described for poly(ethylene glycol) (PEG). While dextran hydrogels have been studied as drug delivery vehicles [24,43], they have not, to the best of our knowledge, been investigated as scaffolds for tissue engineering. This may be explained by previously synthesized dextran hydrogels having morphologies with pores too small for cell penetration and regeneration.

For scaffold utility, the pore size, porosity and interconnectivity become important parameters for analysis where macropores (>50 nm, <300 μm) [44] are most useful for cell and tissue penetration, and smaller pores, such as micropores (<2 nm) and mesopores (>2 nm, <50 nm) [44], contribute to solute diffusion. Previously crosslinked methacrylated dextran hydrogels had very small pores, with diameters up to a few hundred nm [45,46]. Hydrogels obtained by the copolymerization of dextran-allyl isocyanate and poly(*N*-isopropylacrylamide) showed pores with an average diameter of 0.8–3.5 μm [47], which is significantly larger than those of methacrylated dextran, but likely too small for tissue-engineering applications. More recently, Zhang et al. synthesized a macroporous, pH-sensitive *N*-isopropylacrylamide (NIPAAm)/Dex-MA hydrogel with average pore diameters ranging from 3 to 13 μm [48]; however to introduce macroporosity, significantly more NIPAAm vs. Dex-MA was required.

Our goal was to create an open cell, interconnected macroporous dextran hydrogel and to determine the polymerizing conditions of Dex-MA that would lead to the formation of this scaffold. We took advantage of liquid–liquid phase separation caused by polymer–polymer immiscibility in aqueous solutions to create our dextran scaffolds, building on the phenomenon previously described to create dextran microspheres using highly concentrated PEG solutions [49–51]. By careful analysis of the reaction conditions, through the use of formulation phase diagrams, and characterization of the resulting morphologies, we were able to predict the morphology of the resulting scaffold.

2. Materials and methods

2.1. Materials

All chemicals were purchased from Sigma-Aldrich Canada Ltd. (Oakville, Ont.) and used as received, unless otherwise noted. Water was distilled and deionized using Millipore Milli-RO 10 Plus at 18 MΩ resistance. Aqueous solutions of ammonium persulfate (APS) and tetramethylethylene diamine (TEMED) were prepared prior to every use.

2.2. Synthesis of methacrylated dextran (Dex-MA)

The modification of dextran through the addition of GMA was adapted from a methodology previously described [35] using dextran with a molar mass of either 40 or 6 kDa. Briefly, 5 g of dextran (*Leuconostoc mesenteroides*) was dissolved under nitrogen in 50 ml of anhydrous dimethylsulfoxide (DMSO) after which 1 g of 4-dimethylaminopyridine (DMAP) was added. Following the dissolution of DMAP, GMA was added to the solution. For example, 210, 688 or, 1680 μl of GMA was added to achieve a DS of 5, 10 or, 40, respectively. The mixture was stirred at room temperature for 48 h. The reaction was terminated by adding an equimolar amount of concentrated hydrochloric acid (HCl) to neutralize the DMAP. The dextran

solution was extensively dialyzed against distilled water at 4 °C, lyophilized and stored at −20 °C.

The DS was determined by proton nuclear magnetic resonance (^{1}H-NMR) performed on a Gemini 300 MHz spectrometer (Varian Associates, Inc. NMR Instruments, Palo Alto, CA) using D_2O as solvent at 4.8 ppm as the reference. The relevant peaks were integrated to calculate the DS of Dex-MA using the following equation [37]:

$$\mathrm{DS} = \frac{I_\mathrm{B}}{1.04\, I_\mathrm{A}} \times 100, \tag{1}$$

where I_B is the average integrated region of the double bond protons around δ 6 ppm, I_A the integrated area of the anomeric proton of dextran at 5 ppm, and 1.04 the correction factor on the average 4% of α-1, 3 linkages in dextran [35].

2.3. Preparation of Dex-MA scaffolds

Crosslinked Dex-MA hydrogel scaffolds were prepared in tubular-shaped glass molds with excess water in the presence of PEG (M_w of 10 kDa). Varying concentrations of dextran and PEG were dissolved in water. The solution was vortexed for 2 min. The polymerization was initiated by adding 10 wt% APS and 1.4 wt% TEMED (where the wt% of the initiator is relative to the mass of GMA coupled to Dex-MA). The solution was briefly vortexed again and subsequently injected into the glass mold, displacing all of the air within the mold. The mold was plugged and placed in the chuck of a horizontally mounted, variable-speed stirring drill. The polymerization was carried out under barreling at 40 rpm to prevent sedimentation of the dextran phase inside the glass mold, and overnight to minimize any residual amount of non-reacted methacrylated moieties. All scaffolds were washed with deionized water and were allowed to swell in water for 1 week, with daily water exchanges.

2.4. Characterization of Dex-MA scaffolds

2.4.1. Morphology

A scanning electron microscope (SEM) was used to examine the scaffold morphology. Cross-sections of Dex-MA hydrogels were mounted onto aluminum studs and sputter-coated with gold. They were examined under the SEM (S570, Hitachi, Inc., Mountain View, CA) at an accelerating voltage of 20 kV and a working distance of 15 mm.

2.4.2. Equilibrium water content

Hydrogel rods prepared from different DEX-MA/PEG/water formulations were allowed to swell in deionized water for 1 week, with daily water exchanges, in order to reach equilibrium. The rods were weighed to determine the equilibrium hydrated mass. The dry mass was obtained for each rod by freeze-drying the hydrogels and subsequently measuring the mass. The equilibrium water content (EWC) was calculated according to the following equation:

$$\mathrm{EWC} = \frac{w_\mathrm{h} - w_\mathrm{d}}{w_\mathrm{h}} \times 100\%, \tag{2}$$

where w_h is the hydrated mass and w_d the dry mass of the Dex-MA hydrogels.

2.4.3. Interconnected porosity

Diffusion of two proteins, bovine serum albumin (BSA, M_w: 67,000 kDa and immunoglobulin G (IgG, M_w: 1,50,000 kDa), were used to probe the pore interconnectivity of a series of Dex-MA scaffolds by comparing the effective diffusion coefficient, $D_\mathrm{eff,}$ of the proteins in the scaffolds to their diffusion coefficient in free water, D_0. This study was performed on Dex-MA scaffolds obtained by polymerizing Dex-MA 40 kDa DS5 and 6 kDa DS10 in the presence of 0, 2.5 and 5 wt% PEG solutions.

Dex-MA scaffolds were cut in 5-mm rods, loaded with proteins by immersing the scaffolds in 10 mM PBS solution (pH 7.2, 0.02% sodium azide) containing either 5 mg/ml BSA or 0.5 mg/ml IgG. The hydrogel scaffolds were incubated at 37 °C for 1 week to allow the protein solution to equilibrate into the scaffolds and then rinsed in PBS to remove externally adsorbed proteins. The diameter of the scaffolds was measured prior to immersing the samples in 10 ml of 10 mM PBS (pH 7.2, 0.02% sodium azide) at 37 °C. Periodically, 1 ml aliquots were removed and replaced with fresh buffer. The protein concentration of the aliquots was measured with the Bio-rad protein assay using the micro-assay procedure [52].

The concentration of protein loaded in the scaffolds was determined by subtraction of the protein concentration in the solution after one week of scaffold immersion from the initial protein concentration in solution.

Based on the free-volume theory, D_eff was calculated from cumulative release plots. The D_eff values were estimated using the following equation valid for monolithic devices with cylindrical geometry and for $M_t/M_\infty \leqslant 0.4$ [53]:

$$\frac{M_t}{M_\infty} = 4\left(\frac{D_\mathrm{eff}\, t}{\pi r^2}\right)^{1/2}, \tag{3}$$

where M_t is the cumulative amount of released protein at time t, M_∞ the amount of protein originally present in the scaffold, and r the radius of the hydrogel cylinder at equilibrium. The D_eff of the protein in the scaffold is equal to the D_0 divided by the tortuosity (τ), which has a value between 2 and 6 [54]

$$D_\mathrm{eff} = D_0/\tau. \tag{4}$$

2.4.4. Pore size

The pore size distribution of freeze-dried Dex-MA scaffolds was determined by mercury intrusion porosimetry using a Poresizer 9310 (Micromeritics Instrument Corporation, Norcross, GA). The pore diameter, D, was calculated using the Wasburn equation [55]:

$$D = -\frac{4\gamma \cos\theta}{P}, \tag{5}$$

where P is the applied pressure; θ, the contact angle of mercury on the surface of a solid sample (commonly accepted at 140°) and provided by the analytical laboratory and γ the surface tension of mercury (484 dyn cm^{-1}). In order to determine the pore distribution domains of the hydrogel, the critical pressure P_c, i.e. the minimum pressure required to intrude the largest pore, was determined by plotting the following eqation [56]:

$$\ln[V(\infty) - V(P)] = \ln[V(\infty) - V(P_\mathrm{c})] - m[\ln(P) - \ln(P_\mathrm{c})], \tag{6}$$

where $V(\infty)$ is the volume of intruded mercury at the maximum intrusion pressure, $V(P)$ the volume of intruded mercury at pressure P and m the slope of the graph resulting from Eq. (6).

3. Results and discussion

3.1. Dex-MA synthesis

Dex-MA was synthesized by coupling GMA to dextran using an experimental methodology adapted from van Dijk-Wolthuis et al. [35,36]. The ^{1}H-NMR spectrum for Dex-MA (Fig. 1(b)) showed the distinctive resonance peaks of chemically modified dextran through the coupling of GMA. The anomeric proton from the glucopyranosal ring was found at δ 5.0 ppm. The proton at δ 5.3 ppm was from the anomeric carbon due to α-1,3 linkages. Signals from the methacryloyl group were seen at δ 1.95 ppm for the methyl protons and at δ 5.75 and δ 6.2 ppm for the protons at the double bond. The degree of substitution (DS) of GMA coupled to the dextran was quantitatively determined by ^{1}H-NMR, according to Eq. (1), using the integrated areas of the relevant

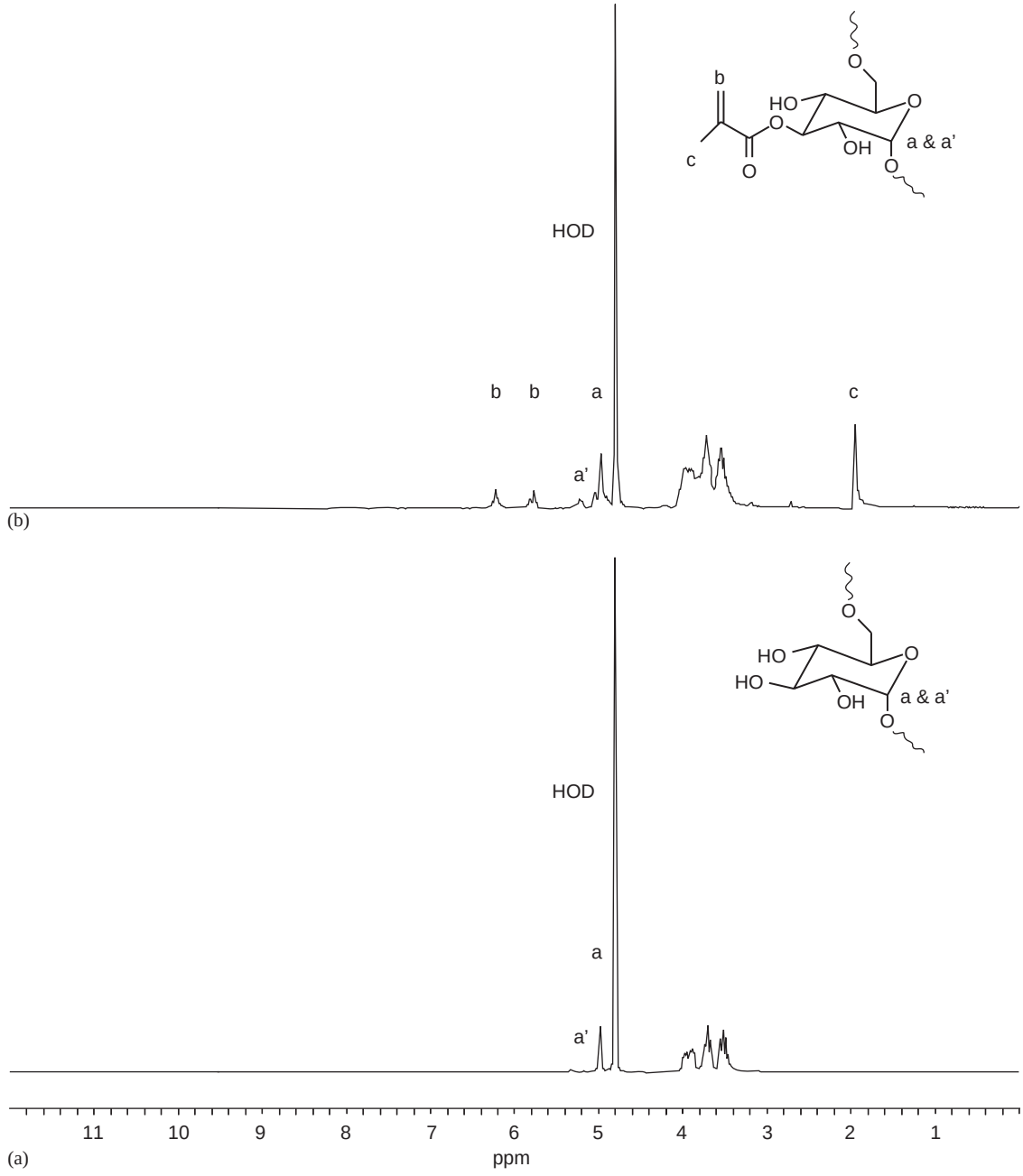

Fig. 1. ^{1}H NMR spectra of: (a) dextran 40 kDa, and (b) Dex-MA 40 kDa DS 40, dissolved in D_2O.

chemical shifts. The following substituted Dex-MA were successfully synthesized: dextran with molar mass of 40 kDa substituted with 5% GMA (Dex-MA 40 kDa DS5) substituted with 40% GMA(Dex-MA 40 kDa DS40) and, dextran with molar mass of 6 kDa modified with 10% GMA (Dex-MA 6 kDa DS10).

3.2. Dex-MA scaffolds

While dextran hydrogels have been previously synthesized, the pores were likely too small for tissue engineering applications [45–47]. Our goal was to create macroporous dextran scaffolds. We adapted the process of Stenekes et al. [50,51] used to synthesize Dex-MA microspheres to prepare Dex-MA scaffolds by taking advantage of the phase separation of Dex-MA from aqueous PEG solutions. To obtain microspheres, they polymerized Dex-MA solution in the presence of a PEG solution under emulsion conditions, which favored the separation of PEG and Dex-MA phases.

3.2.1. Morphology of Dex-MA scaffolds

We investigated the effect of PEG concentration on the morphology of Dex-MA hydrogel scaffolds that were polymerized in mono-phasic conditions. The morphology of these Dex-MA hydrogels is shown in Fig. 2. The SEM micrographs clearly illustrate the dependence of hydrogel morphology on the presence of PEG in the initial solution. As shown in Fig. 2, for 10 wt% Dex-MA 40 kDa DS5 crosslinked in the presence of a PEG 10 kDa solution, the concentration of PEG in solution dramatically affected the pore structure

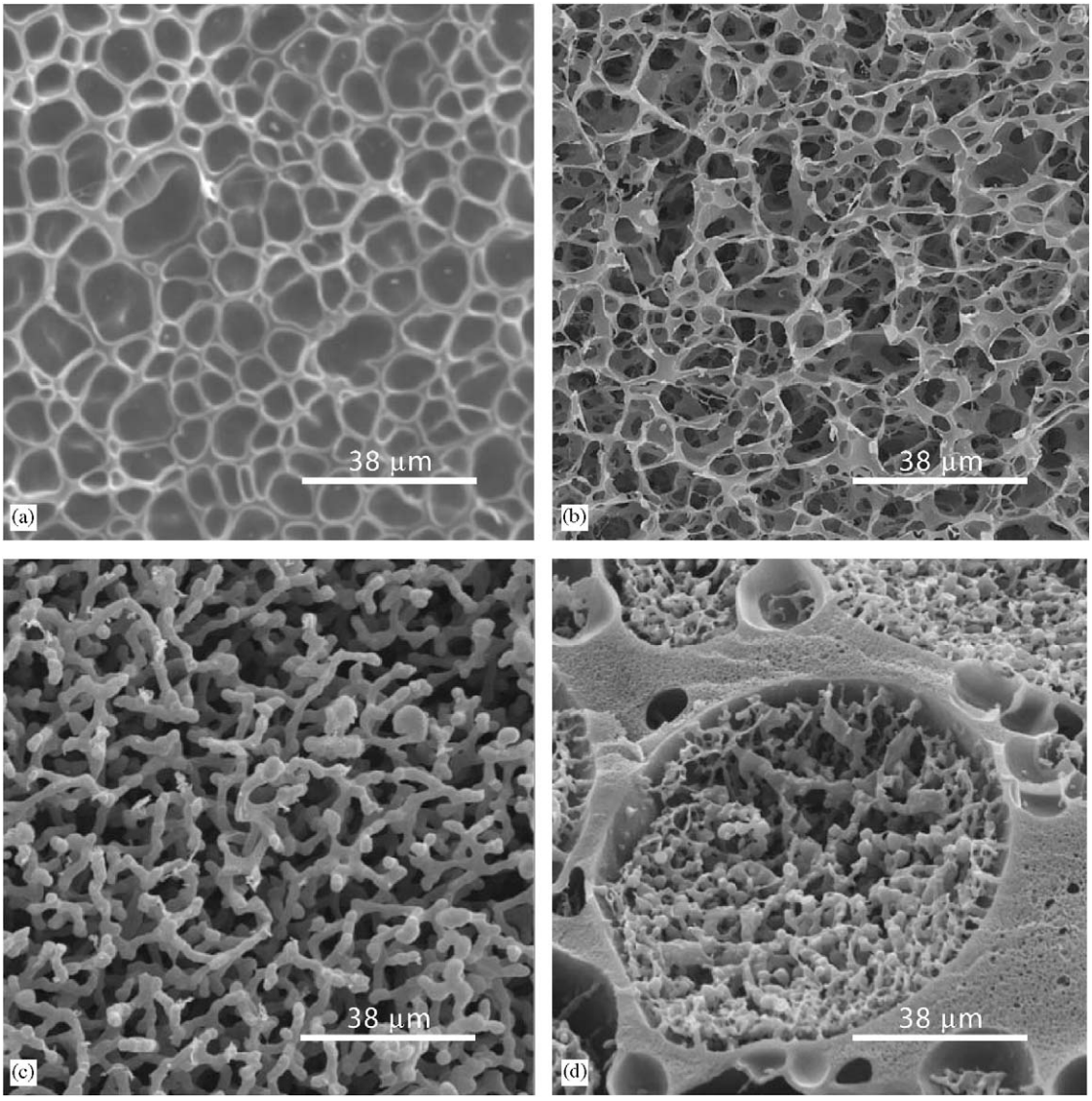

Fig. 2. Representative scanning electron micrographs of crosslinked 10 wt% Dex-MA 40 kDa DS5 scaffolds synthesized in presence of PEG 10 kDa solutions: (a) 0 wt% PEG, (b) 2.5 wt% PEG, (c) 5 wt% PEG and (d) 25 wt% Dex-MA; 5 wt% PEG.

of the resulting Dex-MA gels from microporous with closed pores to macroporous with open pores as PEG concentration increased from 0 to 2.5 wt% (Fig. 2a, b). For 5 wt% PEG, the resulting scaffold had a homogeneous morphology of interconnected beads of approximately 5 μm in diameter (Fig. 2c). Interestingly, this scaffold had a structure similar to those obtained by spinodal decomposition [57], which may also account for the morphology observed during the polymerization of our system. The morphology of polyacrylamide gels polymerized in the presence of varying amounts of PEG has also been attributed to spinodal decomposition [58]. At either higher Dex-MA concentration (25 wt%) or higher PEG concentration (>5 wt%), the polymerization led, respectively, into a heterogeneous scaffold morphology (Fig. 2d) and a heterogeneous suspension (not shown). The hydrogel with an interconnected beaded-wall structure, obtained with 10 wt% Dex-MA 40 kDa DS5 and 5 wt% PEG, was further investigated because of its interesting homogeneous morphology, high pore interconnectivity and pore size.

3.2.2. Mechanism to interconnected beaded Dex-MA scaffolds

In Fig. 3, we propose a mechanism that led to the interconnected beaded scaffold morphology. Initially, Dex-MA and PEG were co-dissolved in water forming a homogeneous solution. After addition of an initiator system, the methacrylate groups of Dex-MA polymerized, leading to crosslinked dextran chains. As the molar mass of crosslinked dextran increased, it phase separated out of solution as Dex-MA beads. These particles gelled together to form a hydrogel with homogeneous interconnected beaded-wall morphology and bicontinuous polymer and water phases.

Dex-MA/PEG/H_2O formulation phase diagrams were created to gain greater insight into the effect of the concentrations of PEG and methacrylated dextran on the formation of this desired macroporous beaded geometry, which is depicted by black squares (■) in Figs. 4–6 for Dex-MA 40 kDa DS5 (Fig. 4), Dex-MA 40 kDa DS40 (Fig. 5), Dex-MA 6 kDa DS10 (Fig. 6). Three different boundaries were observed: (1) at low Dex-MA concentrations, no polymerization was observed (☆); (2) at high PEG concentrations, the resulting polymerization was a

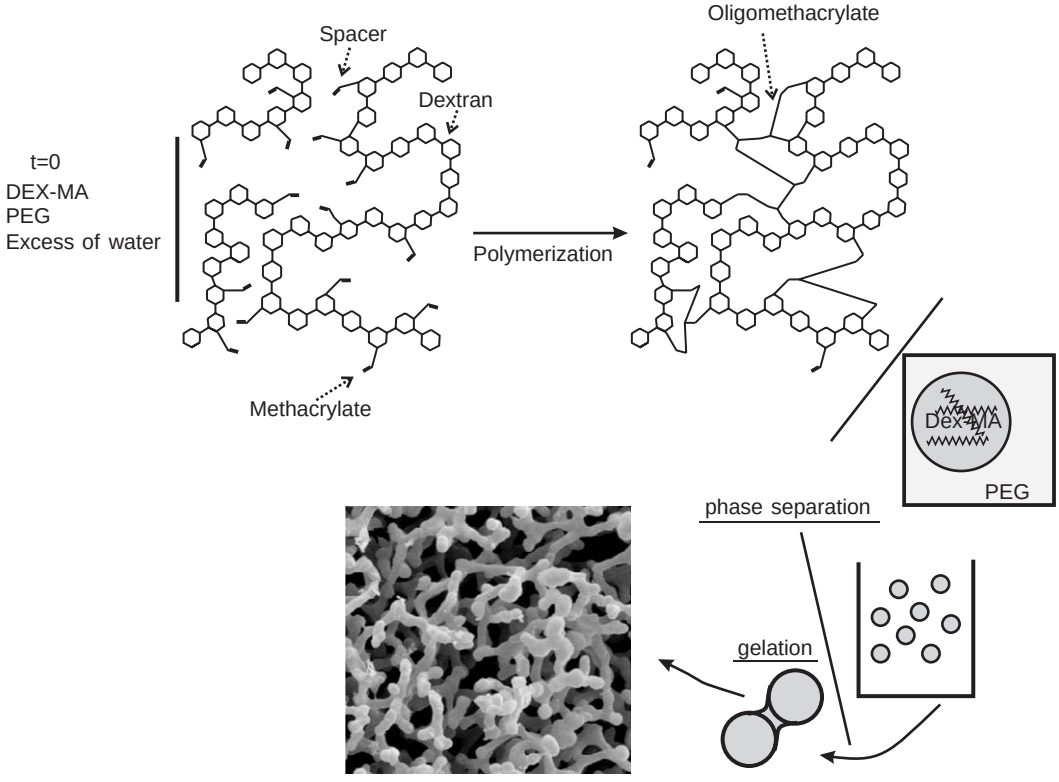

Fig. 3. Illustration of the formation of macroporous beaded dextran hydrogels. Hexagons represent monomer units of dextran and polymerizable groups are represented with " = ". Dex-MA and PEG were dissolved in water forming a homogeneous solution. After the addition of an initiator system, the methacrylate groups of Dex-MA polymerized, leading to crosslinked dextran chains. As the molar mass of dextran increased, it phase separated out of solution as Dex-MA beads. These particles gelled together to form a hydrogel with homogeneous interconnected beaded-wall morphology.

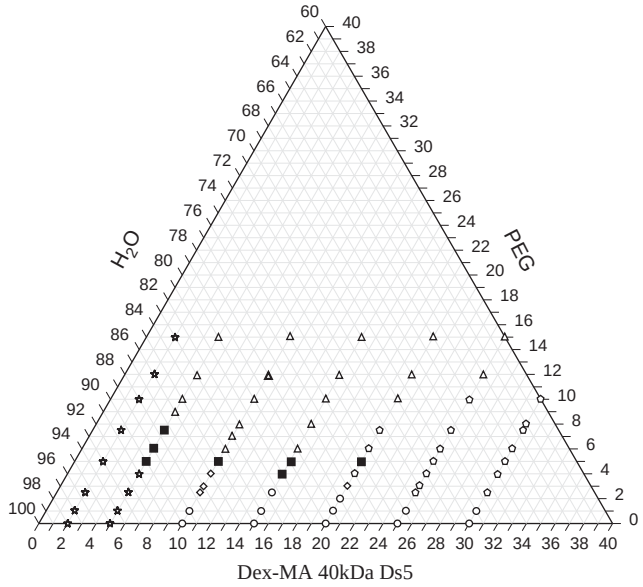

Fig. 4. Phase diagram of Dex-MA 40 DS5.

■  ; ○  ; ◊  ; ⬠  ; ☆ Non-polymerized;

Δ Heterogeneous suspension

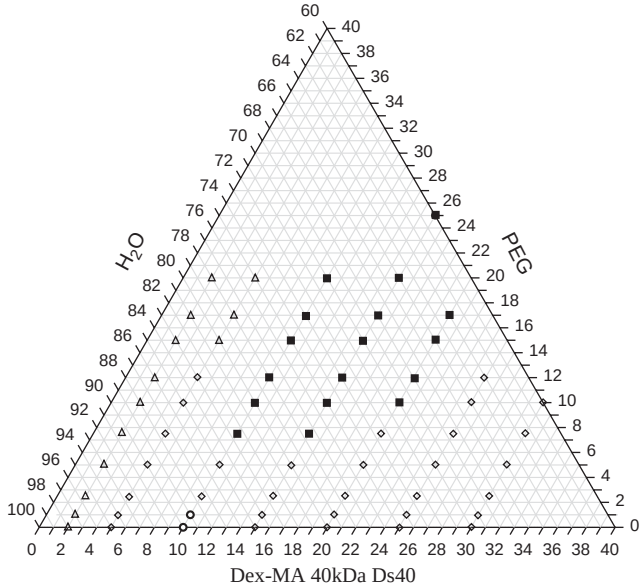

Fig. 5. Phase diagram of Dex-MA 40 kDa DS40.

■  ; ○  ; ◊  ; ⬠  ; ☆ Non-polymerized;

Δ Heterogeneous suspension

heterogeneous suspension (△); and (3) when the solution was very viscous, the structure was heterogeneous (⬠). By varying the ratio of PEG to Dex-MA, the hydrogel geometry changed from microporous gel (○) to a macroporous gel-wall (◊) to a macroporous beaded-wall morphology (■).

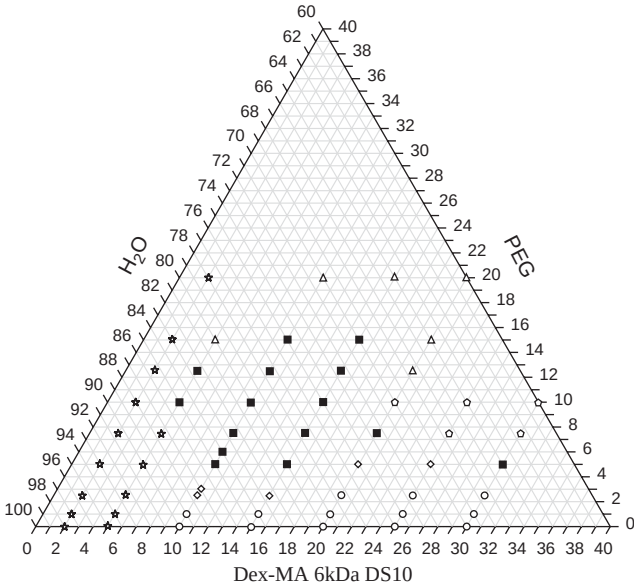

Fig. 6. Phase diagram of Dex-MA 6 kDa DS10.

■  ; ○  ; ◊  ; ⬠  ; ☆ Non-polymerized;

Δ Heterogeneous suspension

These phase diagrams were used to identify the formulations that led to the formation of macroporous beaded scaffold morphologies and based on these results it was possible to extrapolate the morphology that would be obtained from a specific formulation. The beaded structures for Dex-MA 6 kDa DS 10 were obtained with dextran concentrations from 5 to 30 wt% vs. for Dex-MA 40 kDa DS 5 with dextran concentrations from 5 to 20 wt% vs. for Dex-MA 40 kDa DS 40 with dextran concentrations from 10 to 20 wt%. Interestingly as Dex-MA molar mass decreased and Dex-MA DS increased, the number of possible formulations that resulted in the desired macroporous beaded morphology increased. These may be explained by a binodal shift in the phase diagram to higher PEG/Dex-MA concentrations as was described by Stenekes et al. [51] with increasing DS and decreasing molecular weight of Dex-MA.

The macroporous beaded-wall morphology was reproducible with different Dex-MA molar masses and degrees of substitution for Dex-MA of both 40 kDa DS5 (Fig. 7a) and 6 kDa DS10 (Fig. 7b). However, conditions for which the beaded structure was observed were different depending on the DS and M_w of Dex-MA. Dex-MA 40 kDa DS40 (with a higher DS) had smaller macropores (Fig. 7c, d) than Dex-MA 40 kDa DS 5 and 6 kDa DS10 likely because the higher crosslink density of the former led to faster phase separation of the polymerizing solution and smaller pores. While several

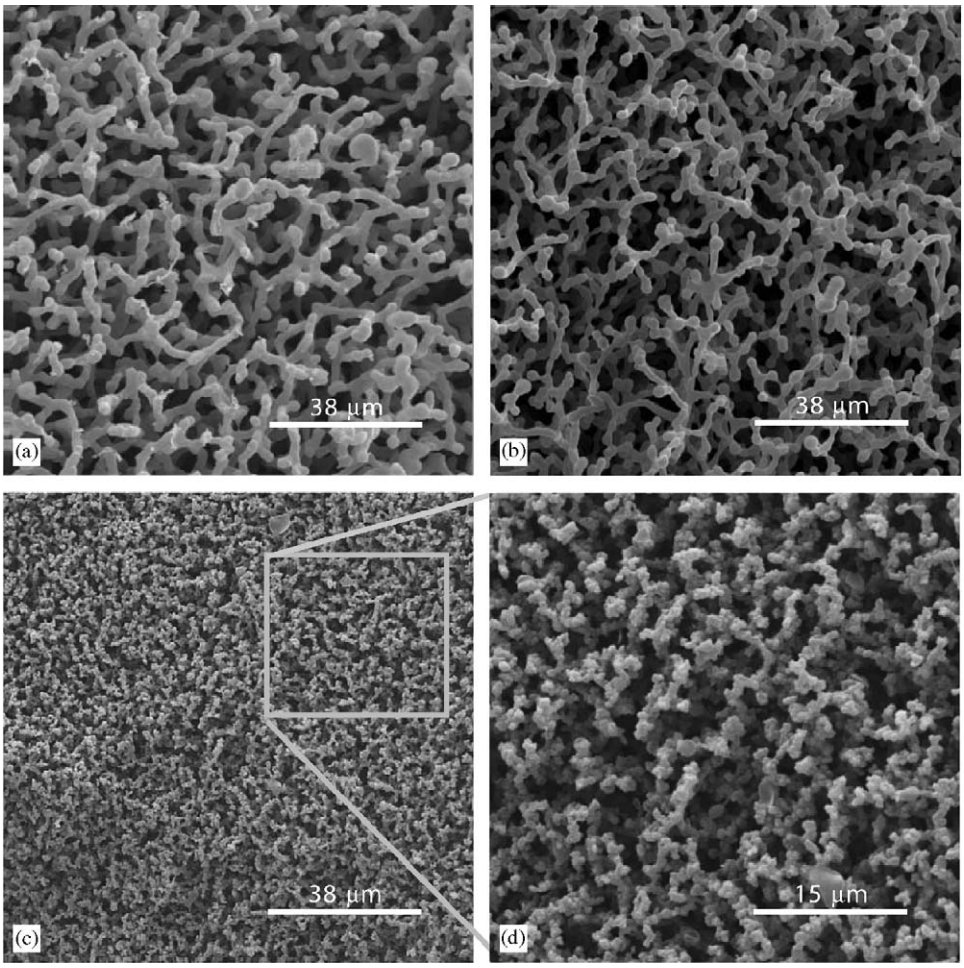

Fig. 7. Scanning electron micrographs of Dex-MA scaffolds of macroporous beaded Dex-MA scaffolds: (a) 10 wt% Dex-MA 40 kDa DS5; 5 wt% PEG, (b) 10 wt% Dex-MA 6 kDa DS10; 5 wt% PEG, and (c, d) 10 wt% Dex-MA 40 kDa DS40; 10 wt% PEG.

formulations led to the beaded structure with both Dex-MA 40 kDa DS 5 and Dex-MA 6 kDa DS 10, the latter is more appealing for scaffold applications because there is a wider range of possible formulations that lead to the desired macroporous interconnected-beaded structure.

3.3. Equilibrium water content

Hydrogels prepared from different Dex-MA/PEG/H_2O formulations were allowed to swell in deionized water for 1 week and the EWC was determined using Eq. (2), the results of which are summarized in Tables 1 and 2. For all the scaffolds obtained with 10 wt% Dex-MA and different PEG concentrations in the polymerizing solution (Table 1), the EWC was between 89% and 94% and was not significantly affected by the change in morphology, whether it was microporous, macroporous with open pores, or a macroporous beaded morphology. When comparing the water content of scaffolds with macroporous beaded morphology obtained with Dex-MA 40 kDa DS 5, Dex-MA 40 kDa DS 40, and Dex-MA 6 kDa DS 10, the EWC of these hydrogels was found to be statistically different ($p<0.001$) yet within a narrow range with values of $91.7\pm0.2\%$, $89.0\pm0.1\%$ and, $95\pm0.1\%$, respectively. Table 2 shows the EWC for Dex-MA 40 kDa DS5 and DS40 when the interconnected beaded geometry was obtained with different

Table 1
Equilibrium water content (EWC) of Dex-MA hydrogels obtained with different PEG concentrations and 10 wt% Dex-MA in the polymerizing solution ($n = 3$, mean $\pm$ standard deviation)

PEG (wt%)	EWC (%)		
	Dex-MA 40 kDa DS5	Dex-MA 40 kDa DS40	Dex-MA 6 kDa DS 10
0	93.2 ± 0.3	89.8 ± 0.4	94.0 ± 0.2
1	93.0 ± 0.9	89.5 ± 0.1	92.9 ± 0.2
2.5	92.8 ± 0.2	88.8 ± 0.5	93.2 ± 0.2
5	91.7 ± 0.2	89.8 ± 0.4	95.0 ± 0.1
10		89.0 ± 0.1	
20		90.0 ± 0.4	

concentrations of Dex-MA in the hydrogel formulation while keeping the PEG concentration constant at 5 and 10 wt%, respectively. For both Dex-MA series, the hydrogels showed a decrease in EWC with an increase of the Dex-MA wt% although the interconnected beaded-wall morphology of these hydrogels was similar under SEM.

3.4. Interconnectivity

The hydrogels with macroporous beaded wall structures were characterized by protein diffusivity to determine the interconnectivity of the pores. BSA (67 kDa) and IgG (150 kDa) were selected to probe the pore interconnectivity of the Dex-MA scaffolds with different morphologies by comparing the effective diffusion coefficient, D_{eff}, of the proteins relative to their diffusion coefficient in water, D_0. D_{eff} of the two proteins were determined according to Eq. (3) and compared to D_0 of BSA (5.9×10^{-7} cm^2/s) and IgG (4.0×10^{-7} cm^2/s) (Table 3) [59,60]. D_{eff} of BSA and IgG decreased in the Dex-MA scaffolds, but was most similar to D_0 for scaffolds having a macroporous beaded wall structure, where D_{eff} was $3.1 \pm 0.2 \times 10^{-7}$ cm^2/s (for BSA) and $1.1 \pm 0.2 \times 10^{-7}$ cm^2/s (for IgG) in Dex-MA 40 kDa DS5 scaffolds. Similar results were obtained for Dex-MA 6 kDa DS10 hydrogel scaffolds, as summarized in Table 4. The change in morphology is accurately represented by the change in D_{eff} measured. Since diffusion in the macroporous interconnected beaded-wall scaffolds is similar to that in water, these scaffolds likely have bicontinuous water and polymer phases with interconnected pores, which increased our interest into this type of hydrogel for tissue-engineering applications.

Table 2
Equilibrium water content (EWC) of interconnected beaded-wall hydrogels obtained with different Dex-MA concentrations ($n = 3$, mean ± standard deviation)

Dex-MA (wt%)	EWC (%)	
	Dex-MA 40 kDa DS5 5 wt% PEG	Dex-MA 40 kDa DS40 10 wt% PEG
5	95.2 ± 0.2	90.2 ± 0.2
10	91.7 ± 0.2	89.0 ± 0.1
15	89.0 ± 0.2	84.3 ± 0.2
20	85.9 ± 0.3	

3.5. Porosity

Different Dex-MA/PEG/H_2O formulations resulted in the formation of hydrogels composed of bicontinuous polymer and water phases. SEM analyses showed that the hydrogels had the desirable homogeneous macroporous beaded-wall morphology. Mercury intrusion porosimetry was used to determine the pore size distribution of these interconnected beaded wall scaffolds and showed a bimodal distribution composed of macropores interconnected by throats. The size distribution of the macropores was very broad irrespective of the formulation, from 10 to 120 μm, with a median pore diameter of 41 ± 9 μm. These pores were connected by tortuous throats, which were also broad, from 5 to 20 μm, with a median diameter of 11 ± 1 μm. These results, in combination with the interconnectivity data, suggest that the macroporous beaded-wall hydrogels have a morphology suitable for tissue engineering.

Table 3
Effective diffusion coefficients of BSA ($D_{eff,\ BSA}$) and IgG ($D_{eff,\ IgG}$) in Dex-MA 40 kDa DS5 scaffolds ($n = 3$, mean ± standard deviation)

Hydrogel	$D_{eff,\ BSA} \times 10^7$ (cm^2/s)	$D_{eff,\ IgG} \times 10^7$ (cm^2/s)
Water	5.9 [59]	4.0 [60]
Microporous structure with close pores 10% Dex-MA 40 kDa D 5, 0% PEG	0.21 ± 0.01	0.16 ± 0.02
Macroporous gel-wall structure 10% Dex-MA 40 kDa DS 5, 2.5% PEG	1.5 ± 0.2	0.46 ± 0.05
Macroporous-beaded structure 10% Dex-MA 40 kDa DS 5, 5% PEG	3.1 ± 0.2	1.11 ± 0.2

Table 4
Effective diffusion coefficients of BSA ($D_{eff,\ BSA}$) and IgG ($D_{eff,\ IgG}$) in Dex-MA 6 kDa DS10 scaffolds ($n = 3$, mean ± standard deviation)

Hydrogel	$D_{eff,\ BSA} \times 10^7$ (cm^2/s)	$D_{eff,\ IgG} \times 10^7$ (cm^2/s)
Water	5.9 [59]	4.0 [60]
Microporous structure with close pores 10% Dex-MA 6 kDa DS 10, 0% PEG	0.6 ± 0.1	0.29 ± 0.02
Macroporous gel-wall structure 10% Dex-MA 6 kDa DS 10, 2.5% PEG	0.8 ± 0.2	0.31 ± 0.05
Macroporous-beaded structure 10% Dex-MA 6 kDa DS 10, 5% PEG	1 ± 0.2	0.96 ± 0.02

4. Conclusions

Crosslinked dextran hydrogels were synthesized by radical polymerization of methacrylate groups coupled to dextran, yielding a crosslinked network. By controlling the liquid–liquid phase separation caused by immiscibility of Dex-MA and PEG in aqueous solutions, macroporous, interconnected beaded wall morphology scaffolds were created. The presence of PEG in solution had a significant effect on the final morphology of the dextran hydrogel leading to the formation of different types of structures, from microporous gel to macroporous gel-wall to a macroporous interconnected-beaded structure.

Dex-MA/PEG/H_2O formulation diagrams for the different Dex-MA synthesized allowed us to determine the conditions for which the macroporous interconnected beaded structure could be obtained. We believe that porous hydrogels with a macroporous interconnected beaded structure are important for scaffolds used in tissue engineering applications to facilitate cell penetration, nutrient diffusion, and tissue regeneration. In ongoing studies, we are investigating cell penetration in, and cell interaction with, these scaffolds and the importance of peptide modification thereof to this end.

Acknowledgements

We are grateful to Irene Ying for performing some of the protein diffusion experiments and to Prof. Ioannis Chatzis for use of his mercury porosimeter (Department of Chemical Engineering, University of Waterloo). We thank the Natural Sciences and Engineering Research Council of Canada (MSS) and the Fonds québécois de la recherche sur la nature et les technologies (SGL) for financial support.

References

[1] Zekorn TD, Horcher A, Mellert J, Siebers U, Altug T, Emre A, Hahn HJ, Federlin K. Biocompatibility and immunology in the encapsulation of islets of Langerhans (bioartificial pancreas). Int J Artif Organs 1996;19(4):251–7.

[2] Gombotz WR, Pettit DK. Biodegradable polymers for protein and peptide drug delivery. Bioconjug Chem 1995;6(4):332–51.

[3] Peppas NA, Bures P, Leobandung W, Ichikawa H. Hydrogels in pharmaceutical formulations. Eur J Pharm Biopharm 2000;50(1):27–46.

[4] Drury JL, Mooney DJ. Hydrogels for tissue engineering: scaffold design variables and applications. Biomaterials 2003;24(24):4337–51.

[5] Hoffman AS. Hydrogels for biomedical applications. Adv Drug Deliv Rev 2002;54(1):3–12.

[6] Lutolf MP, Lauer-Fields JL, Schmoekel HG, Metters AT, Weber FE, Fields GB, Hubbell JA. Synthetic matrix metalloproteinase-sensitive hydrogels for the conduction of tissue regeneration: engineering cell-invasion characteristics. Proc Natl Acad Sci USA 2003;100(9):5413–8.

[7] Lee KY, Mooney DJ. Hydrogel for tissue engineering. Chem Rev 2001;101:1869–79.

[8] Gotoh T, Honda H, Shiragami N, Unno H. A new type porous carrier and its application to culture of suspension cells. Cytotechnology 1993;11(1):35–40.

[9] Shapiro L, Cohen S. Novel alginate sponges for cell culture and transplantation. Biomaterials 1997;18:583–90.

[10] Rowley JA, Madlambayan G, Mooney DJ. Alginate hydrogels as synthetic extracellular matrix materials. Biomaterials 1999;20:45–53.

[11] Dvir-Ginzberg M, Gamlieli-Bonshtein I, Agbaria R, Cohen S. Liver tissue engineering within alginate scaffolds: effects of cell-seeding density on hepatocyte viability, morphology, and function. Tissue Eng 2003;9(4):757–66.

[12] Eiselt P, Yeh J, Latvala RK, Shea LD, Mooney DJ. Porous carriers for biomedical applications based on alginate hydrogels. Biomaterials 2000;21:1921–7.

[13] Risbud M, Hardikar A, Bhone R. Chitosan-polyvinyl pyrrolidone hydrogels as candidate for islet immunoisolation: in vitro biocompatibility evaluation. Cell Transplant 2000;9(1):25–31.

[14] Zielinski BA, Aebisher P. Chitosan as a matrix for mammalian cell encapsulation. Biomaterials 1994;15(13):1049–56.

[15] Suh JKF, Matthew WT. Application of chitosan-based polysaccharide biomaterials in cartilage tissue engineering: a review. Biomaterials 2000;21:2589–98.

[16] Gentleman E, Lay AN, Dickerson DA, Nauman EA, Livesay GA, Dee KC. Mechanical characterization of collagen fibers and scaffolds for tissue engineering. Biomaterials 2003;24(21):3805–13.

[17] Porath J, Flodin P. Gel filtration: A method for desalting and group separation. Nature 1959;183:1657–9.

[18] Bollag D. Gel-filtration chromatography. Methods Mol Biol 1994;36:1–9.

[19] Bollag D. Ion-exchange chromatography. Methods Mol Biol 1994;36:11–22.

[20] Shibusawa Y. Surface affinity chromatography of human peripheral blood cells. J Chromatogr B 1999;722:71–88.

[21] Cunningham J, Hodgson H. Microcarrier culture of hepatocytes in whole plasma for use in liver support bioreactors. Int J Artif Organs 1992;15:162–7.

[22] Pawlowski R, Szigeti V, Loyd R, Przybylski R. Primary culture of chick embryo skeletal muscle on dextran microcarrier. Eur J Cell Biol 1984;35:296–303.

[23] Hirtenstein M, Clark J, Lindgren G, Vretblad P. Microcarriers for animal cell culture: a brief review of theory and practice. Dev Biol Stand 1980;46:109–16.

[24] Hennink WE, Cadee JA, de Jong SJ, Franssen O, Stenekes RJH, Talsma H, van Dijk-Wolthuis WNE. Molecular design of biodegradable dextran hydrogels for controlled release of proteins. In: Chiellini E, Sunamoto J, Migliaresi C, Ottenbrite R, Cohn D, editors. Biomedical polymers and polymer therapeutics. New York: Kluwer Academic/Plenum Publishers; 2001. p. 3–18.

[25] de Jong SJ, De Smedt SC, Whals MWC, Demeester J, Kettenes-van den Bosch J, Hennink WE. Novel self-assembled hydrogels by stereocomplex formation in aqueous solution of enantiomeric lactic acid oligomers grafted to dextran. Macromolecules 2000;33:3680–6.

[26] Hovgaard L, Brondsted H. Dextran hydrogels for colon-specific drug delivery. J Control Release 1995;26:159–66.

[27] Brondsted H, Andersen C, Hovgaard L. Crosslinked dextran—a new capsule material for colon targeting of drugs. J Control Release 1998;53:7–13.

[28] Draye JP, Delaye B, Van de Voorde A, Van Den Bulcke A, De Reu B, Schacht E. In vitro and in vivo biocompatibility of dextran

dialdehyde cross-linked gelatin hydrogel films. Biomaterials 1998;19:1677–87.
[29] Draye JP, Delaey B, Van de Voorde A, Van Den Bulcke A, Bogdanov B, Schacht E. In vitro release characteristics of bioactive molecules from dextran dialdehyde cross-linked gelatin hydrogel films. Biomaterials 1998;19:99–107.
[30] Edman P, Ekman B, Sjoholm I. Immobilization of proteins in microspheres of biodegradable polyacryldextran. J Pharm Sci 1980;69:838–42.
[31] Zhang Y, Won CY, Chu CC. Synthesis and characterization of biodegradable hydrophobic-hydrophilic hydrogel networks with a controlled swelling property. J Polym Sci A 2000;38:2392–404.
[32] Kim SH, Won CY, Chu CC. Synthesis and characterization of dextran-based hydrogel prepared by photocrosslinking. Carbohydrate Polym 1999;40:183–90.
[33] Zhang Y, Chu CC. Biodegradable dextran-polylactide hydrogel networks: their swelling, morphology and the controlled release of indomethacin. J Biomed Mater Res 2002;59:318–28.
[34] Ferreira L, Gil M, Dordick J. Enzymatic synthesis of dextran-containing hydrogel. Biomaterials 2002;23:3957–67.
[35] van Dijk-Wolthuis WNE, Franssen O, Talsma H, van Steenbergen MJ, Kettenes-van den Bosh JJ, Henink WE. Synthesis, characterization, and polymerization of glycidyl methacrylate derivatized dextran. Macromolecules 1995;28:6317–22.
[36] van Dijk-Wolthuis WNE, Kettenes-van den Bosh JJ, van der Kerk-van Hoof A, Hennink W. Reaction of dextran with glycidyl methacrylate: an unexpected transesterification. Macromolecules 1997;30:3411–3.
[37] van Dijk-Wolthuis WNE, Tsang SKY, Kettenes-van den Bosch JJ, Hennink WE. A new class of polymerizable dextrans with hydrolyzable groups: hydroxyethyl methacrylated dextran with and without oligolactate spacer. Polymer 1997;38:6235–42.
[38] van Dijk-Wolthuis WE, Hoogeboom J, van Steenbergen M, Tsang SY, Hennink W. Degradation and release behavior of dextran-based hydrogels. Macromolecules 1997;30:4639–45.
[39] Cadee J, van Luyn M, Brouwer L, Plantinga J, van Wachem P, de Groot C, den Otter W, Hennink W. In vivo biocompatibility of dextran-based hydrogels. J Biomed Mater Res 2000;50:397–404.
[40] McLean KM, Johnson G, Chatelier RC, Beumer GJ, Steele JG, Griesser HJ. Method of immobilization of carboxymethyl-dextran affects resistance to tissue and cell colonization. Colloids Surf B 2000;18:221–34.
[41] McArthur S, McLean K, Kingshott P, St John H, Chatelier R, Griesser H. Effect of polysaccharide structure on protein adsorption. Colloids Surf B 2000;17:37–48.
[42] Massia S, Stark J. Immobilized RGD peptides on surfaces-grafted dextran promote biospecific cell attachment. J Biomed Mater Res 2001;56:390–9.
[43] Trudel J, Massia SP. Assessment of the cytotoxicity of photocrosslinked dextran and hyaluronan-based hydrogels to vascular smooth muscle cells. Biomaterials 2002;23(16):3299–307.
[44] Woerly S. Restorative surgery of the central nervous system by means of tissue engineering using NeuroGel implants. Neurosurg Rev 2000;23:59–77.
[45] Kim SH, Chu CC. Pore structure analysis of swollen dextran-methacrylate hydrogels by SEM and mercury intrusion porosimetry. J Biomed Mater Res (Appl Biomater) 2000;53:258–66.
[46] Stenekes RJ, De Smedt SC, Demeester J, Sun G, Zhang Z, Hennink WE. Pore sizes in hydrated dextran microspheres. Biomacromolecules 2000;1(4):696–703.
[47] Zhang XZ, Wu DQ, Sun GM, Chu CC. Novel biodegradable and thermosensitive Dex-AI/PNIPAAm hydrogel. Macromol Biosci 2003;3(2):87–91.
[48] Zhang XZ, Wu DQ, Chu CC. Synthesis and characterization of partially biodegradable, temperature and pH sensitive Dex-MA/PNIPAAm hydrogels. Biomaterials 2004;25:4719–30.
[49] Franssen O, Jennink WE. A novel preparation method for polymeric microparticles without the use of organic solvents. Int J Pharm 1998;168:1–7.
[50] Stenekes RJH, Franssen O, van Bommel EMG, Crommelin DJA, Hennink WE. The use of aqueous PEG/dextran phase separation for preparation of dextran microspheres. Int J Pharm 1999;183:29–32.
[51] Stenekes RJH, Franssen O, van Bommel EMG, Crommelin DJA, Hennink WE. The preparation of dextran microspheres in an all-aqueous system: effect of the formulation parameters on particle characteristics. Pharm Res 1998;15:557–61.
[52] Bradford M. A rapid and sensitive method for the quantitation of microgram quantities of protein utilizing the principle of protein-dye binding. Anal Biochem 1976;72:248–54.
[53] Hennink WE, Talsma H, Borchert JCH, De Smedt SC, Demeester J. Controlled release of proteins from dextran hydrogels. J Control Release 1996;39:47–55.
[54] Cussler EL. Diffusion-mass transfer fluid systems. Cambridge: Cambridge University Press; 1984.
[55] Washburn EW. The dynamics of capillary flow. Phys Rev 1921;17:273–83.
[56] Woerly S, Pinet E, De Robetis L, Bousmina M, Laroche G, Roitback T, Vargova L, Sykova E. Heterogeneous PHPMA hydrogels for tissue repair and axonal regeneration in the injured spinal cord. J Biomater Sci Polymer Ed 1998;9:681–711.
[57] Inoue T. Reaction-induced phase decomposition in polymer blends. Prog Polym Sci 1995;20:119–53.
[58] Asnaghi D, Giglio M, Bossi A, Righetti PG. Large-scale microsegregation in polyacrylamide gels (spinodal gels). J Chem Phys 1995;102:9736–42.
[59] Merrill EW, Dennison KA, Sung C. Partitioning and diffusion of solutes in hydrogels of poly(ethylene oxide). Biomaterials 1993;14:1117–26.
[60] Burczak K, Fujisato T, Hatada M, Ikada Y. Protein permeation through poly(vinyl alcohol) hydrogel membranes. Biomaterials 1994;15:231–8.